Probing the Electronic Structures and Relative Stabilities of Monomagnesium Oxide Clusters MgOx− and MgOx (x=1−4): A Combined Photoelectron Imaging and Theoretical Investigation

ARTICLE *in* THE JOURNAL OF PHYSICAL CHEMISTRY A · MAY 2013

Impact Factor: 2.69 · DOI: 10.1021/jp403134g · Source: PubMed

4 AUTHORS, INCLUDING:

Shibo Cheng
Pennsylvania State University
19 PUBLICATIONS **75** CITATIONS
SEE PROFILE

Cuneyt Berkdemir
Pennsylvania State University
47 PUBLICATIONS **795** CITATIONS
SEE PROFILE

Joshua Melko
University of North Florida
38 PUBLICATIONS **188** CITATIONS
SEE PROFILE

THE JOURNAL OF PHYSICAL CHEMISTRY A

Article

pubs.acs.org/JPCA

Probing the Electronic Structures and Relative Stabilities of Monomagnesium Oxide Clusters MgO_x^- and MgO_x (x = 1−4): A Combined Photoelectron Imaging and Theoretical Investigation

Shibo Cheng,[†] Cuneyt Berkdemir,[†] Joshua J. Melko,[†] and A. W. Castleman, Jr.*[,†,‡]

[†]Department of Chemistry and [‡]Department of Physics, The Pennsylvania State University, University Park, Pennsylvania 16802, United States

ABSTRACT: The electronic and structural properties of small monomagnesium oxide clusters, MgO_x^- and MgO_x (x = 1−4), have been investigated using a synergistic approach combining photoelectron imaging spectroscopy and first principles electronic structure calculations. The adiabatic detachment energy (ADE) and vertical detachment energy (VDE) of MgO_x^- clusters along with the photoelectron angular distributions (PADs) are determined experimentally. The measured PADs of the clusters are dependent on both the orbital symmetry and electron kinetic energies. Density-functional theory (DFT) calculations were performed to explore the optimized geometries of neutral and anionic MgO_x clusters. The theoretical ADE and VDE values calculated according to the optimized geometries are in good agreement with our experimental measurements. In addition, MgO^- and MgO_4 clusters are found to have enhanced relative stability in the corresponding anionic and neutral series, based on both theoretical parameters and the experimental cluster distribution.

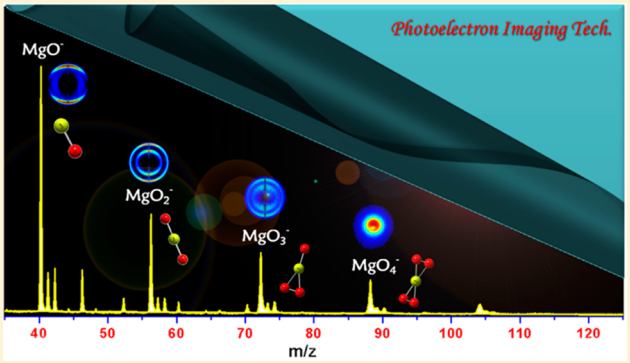

1. INTRODUCTION

As an intermediate form between the bulk and atomic counterparts, clusters have received much attention during the past several decades. A wealth of studies[1−9] has made it clear that the electronic and geometrical properties and stability of clusters can be altered dramatically by changing just one atom or one electron. Such a remarkable phenomenon provides a route to design cluster-assembled nanomaterials with tailored properties that are a function of cluster size and composition. In fact, the formation, growth, and shape control of clusters and nanomaterials have been reported in the synthesis of metals, semiconductors, and metal oxides recently.[10−13] Among various clusters, the interaction between metal atoms and oxygen is of major importance due to the wide usage of oxides in catalytic processes, surface chemistry, and thermite reactions.[14,15] Particularly, the importance of magnesium oxide as an ultrathin oxide film which can be used in catalysis has motivated a wealth of investigations recently.[16−18] Moreover, MgO-based materials have also been used as a sorbent to capture one of the greenhouse gases, carbon dioxide (CO_2).[19−21] It is very important, therefore, to explore the electronic structures and geometries of magnesium oxides at the molecular level, which can help design better catalysts and provide insights toward isolating/depositing these basic building blocks in the condensed phase. Gas-phase oxide cluster studies could provide valuable molecular models for metal oxide surfaces and reveal mechanistic information to surface chemical reactions.[22−32]

There have been a number of previous gas-phase studies on magnesium oxide clusters,[33−38] especially monomagnesium oxide (MgO) cluster which can be considered as the simplest ionic oxide species, crystallizing in the rock salt (NaCl) structure.[39] The vibrationally resolved photoelectron spectra of MgO^- at different photon energies have been recorded by Kim et al. recently, providing detailed information about the low-lying electronic states of MgO and MgO^-.[33] Besides the single MgO molecule, the photoelectron spectra of $(MgO)_x^-$ (x = 1−5) have also been reported by Gutowski et al., showing an unusual decrease of electron binding energy from x = 1 to 4 and a subsequent increase from 4 to 5.[34] Additionally, mass spectra of $(MgO)_x^+$ and $(MgO)_xMg^+$ clusters have been studied by using laser-ionization time-of-flight mass spectrometry.[35,36] It was found that the clusters form compact cubic structures similar to pieces of the MgO crystal lattice, and the most abundant clusters have a $(MgO)_3$ subunit. Moreover, infrared multiphoton ionization/dissociation techniques have also been used to explore the structural properties of the $(MgO)_x$ clusters.[37,38]

Compared with the extensively spectroscopic and catalytic studies on MgO-based clusters, the electronic structures,

Special Issue: Curt Wittig Festschrift

Received: March 29, 2013
Revised: May 20, 2013
Published: May 21, 2013

Table 1. Equilibrium Bond Lengths r_e (in Å) and Vibrational Frequencies ω (in cm^{-1}) of MgO and MgO^- Clusters Calculated with Four Different Methods and Three Basis Sets[a]

		theory							
		6-311++G		aug-cc-pVDZ		aug-cc-pVQZ		experiment	
methods	species	ω	r_e	ω	r_e	ω	r_e	ω	r_e
PBEPBE	^1MgO	750	1.798	793	1.765	807	1.751	780 ± 40[b]	1.749[c]
	$^2MgO^-$	657	1.857	693	1.821	709	1.805	670 ± 80[b]	1.794[b,c]
,[c]B3LYP	^3MgO	597	1.950	609	1.902	617	1.889		
	$^2MgO^-$	636	1.853	685	1.814	701	1.797		
HF	^3MgO	629	1.916	678	1.874	683	1.859		
	$^4MgO^-$	572	1.952	618	1.902	630	1.882		
MP2	^1MgO	989	1.758	1008	1.757	1013	1.743		
	$^2MgO^-$	686	1.863	827	1.847	958	1.838		

[a]Experimental results are also included as a comparison. [b]Experimental data extracted from ref 33. [c]Experimental data extracted from ref 50.

geometries, and relative stability of O-rich MgO_x ($x > 1$) clusters, to the best of our knowledge, have not been investigated systematically. The chemically bound superoxide molecule MgO_2^+ has been studied in a reflectron time-of-flight mass spectrometer over the spectral range 247−540 nm by Chen et al.[40] Theoretically, the spectroscopy and the metastability of the lowest electronic states of *l*-$MgOO^+$ and MgO_2^+ are investigated using high-level computational methods, and the theoretical results are used to propose the mechanism for the $Mg^+ + O_2$ atmospheric ion−molecule reaction.[41] However, there are no gas-phase spectroscopic studies hitherto to explore the electronic structures and relative stability of these O-rich MgO_x clusters, which can serve as valuable molecular models for O_2 adsorption and activation on the Mg center.

In the present work, we report a systematic study of the electronic and structural properties of anionic and neutral monomagnesium oxide (MgO_x (x = 1−4)) clusters by using photoelectron imaging spectroscopy and first principles electronic structure calculations. The photoelectron images were recorded using two different photon energies, 532 nm (2.33 eV) and 355 nm (3.49 eV). The concerted experimental and computational results establish the ground-state structures for anionic and neutral MgO_x clusters. Furthermore, the relative stability in the studied cluster series is discussed based on the energy gain, HOMO−LUMO gap, and fragmentation channels. Based on both experimental and theoretical results, we suggest that MgO^- and MgO_4 clusters are more stable in the corresponding anionic and neutral cluster series studied here.

2. EXPERIMENTAL DETAILS

The experimental setup used in the present work has been described in detail elsewhere,[42−44] and a brief account is as follows. The apparatus consists of a laser vaporization source, a Wiley−McLaren time-of-flight (TOF) mass spectrometer,[45] and a velocity map imaging analyzer.[43] MgO_x^- (x = 1−4) clusters were generated in a laser vaporization cluster source, where the second harmonic output (532 nm) of a Nd:YAG laser was focused on a 1/4″ pure magnesium rod to form a plasma. A high-purity helium carrier gas (typically 50 psi), seeded with 1% N_2O gas and delivered by a 10 Hz pulsed valve, reacted with laser-ablated Mg atoms. The neutral and charged clusters then expanded through a conical nozzle and were collimated by a skimmer. The formed negative ions were perpendicularly extracted and mass-analyzed using a Wiley−McLaren time-of-flight mass spectrometer.[45] Along the time-of-flight path, ions passed through the laser detachment region, where they could be intercepted with the second harmonic (532 nm) or third harmonic (355 nm) output of a Nd:YAG laser, which was linearly polarized parallel to the imaging plane. The resultant photoelectrons were directed toward a detector consisting of a 40 mm diameter microchannel plate (MCP) and a phosphor screen. The two-dimensional (2D) images produced on the phosphor screen were recorded with a charge-coupled device camera. An image acquisition program (Davis) was used to collect the images, which allows summing up of individual laser shots and background subtraction. The three-dimensional (3D) distributions were reconstructed from the photoelectron images using the basis set expansion (BASEX) inverse Abel transform method.[46] The velocity distribution and photoelectron spectra were both obtained from the reconstructed images. The photoelectron spectra were calibrated against the known spectrum of Bi^-.[47]

3. COMPUTATIONAL METHOD

All calculations were performed using the Gaussian 09 program package.[48] The singlet, triplet, and quintet spin multiplicity states of neutral MgO_x (x = 1−4) clusters and the doublet, quartet and sextet spin multiplicity states of anionic MgO_x (x = 1−4) clusters were treated using density functional theory (DFT) as implemented in Gaussian 09. For simplicity, only the lowest spin multiplicity states for the studied clusters are discussed here. To determine the ground-state geometries for the clusters, different initial geometries and spin states were attempted and fully optimized without constraints. Vibrational frequency calculations were also performed to verify the nature of the stationary points, and all structures presented here are true minima. Additionally, the zero-point energy corrections have been included in the total energy results of clusters. In order to find a reliable level of theory as a starting point of this study, we performed an initial calculation to compare the equilibrium bond lengths (r_e) and vibrational frequencies (ω) of MgO and MgO^- with known experimental values reported before.[33,34,49−51] Here, we carried out the test calculations by using the B3LYP,[52] PBEPBE,[53,54] Hartree−Fock (HF), and Moller−Plesset (MP2) methods with the 6-311++G,[55] aug-cc-pVDZ,[56] and aug-cc-pVQZ[57] basis sets. The theoretical r_e and ω values calculated at different methods and basis sets are shown in Table 1, along with the experimental results.[33,34,50] As can be seen from Table 1, the theoretical r_e and ω values of MgO and MgO^- clusters calculated at the PBEPBE/aug-cc-pVQZ level of theory are in good agreement with previous

dx.doi.org/10.1021/jp403134g | J. Phys. Chem. A 2013, 117, 11896−11905

experimental results. The spin multiplicity (M) results are also given for MgO and MgO^- clusters in Table 1 at different levels of theory. The electronic structure of the MgO cluster has been the subject of numerous theoretical[58−61] and experimental[62−64] investigations. Previous experimental[62] and theoretical[58] results have demonstrated that the electronic ground state of MgO is the $^1\Sigma^+$ state. In addition, Kim et al.[33] have assigned the $^2\Sigma^+$ state to be the ground state of MgO^- experimentally. All of these findings are consistent with our spin multiplicity results calculated at the PBEPBE/aug-cc-pVQZ level of theory. Therefore, based on the above-mentioned results given in the test calculations, the PBEPBE/aug-cc-pVQZ level of theory has been chosen to predict the electronic properties of the $MgO_x^{0/-}$ (x = 1−4) clusters. Moreover, in order to get more accurate adiabatic detachment energies (ADEs) and vertical detachment energies (VDEs) of MgO_x^- (x = 1−4) clusters, the electronic energies corresponding to the PBEPBE/aug-cc-pVQZ optimized geometries were refined further through the calculations at the CCSD(T)[65,66] level with the aug-cc-pVQZ basis set.

4. RESULTS AND DISCUSSION

4.1. Photoelectron Spectra and Images of Monomagnesium Oxides MgO_x^- (x = 1−4). The photoelectron images from detachment of MgO_x^- (x = 1−4) clusters as well as the corresponding photoelectron spectra obtained at different photon energies are shown in Figures 1−4,

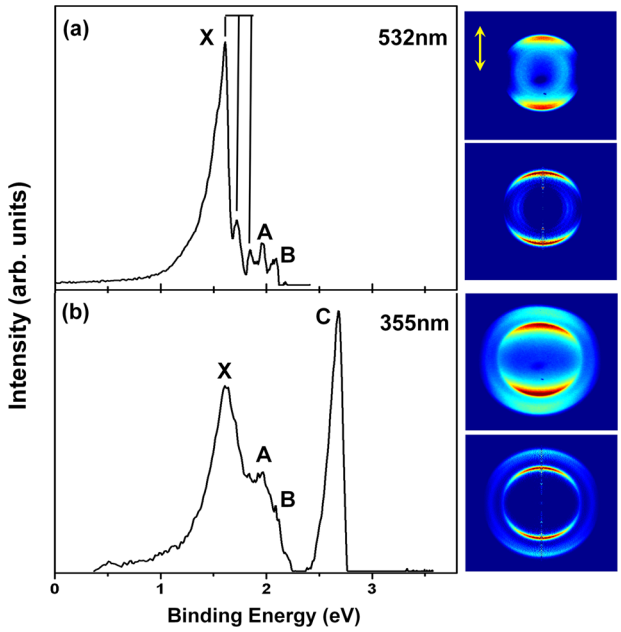

Figure 1. Photoelectron raw images (top on the right), reconstructed images (bottom on the right), and the photoelectron spectra of MgO^- obtained at (a) 532 nm (2.33 eV) and (b) 355 nm (3.49 eV). Laser polarization is vertical in the plane of the page.

respectively. The raw image (top on the right of each spectrum) collected in the experiment shows the projection of the three-dimensional (3D) laboratory frame photoelectron probability density onto the plane of the imaging detector, and the reconstructed image (bottom on the right of each spectrum) represents the central slice of the 3D distribution from its 2D projection. The spectra are plotted on a binding energy scale. The binding energy is defined as

$$e_{BE} = h\nu - e_{KE} \quad (1)$$

where e_{BE} is the electron binding energy, $h\nu$ is the photon energy, and e_{KE} is the kinetic energy of the photodetached electron. The rings in a velocity map image are analogous to peaks in the corresponding photoelectron spectrum. The observed peaks in the photoelectron spectra are labeled with letters, which denote the electronic transitions from the anion ground state to the neutral ground state (band X) and higher neutral excited states (A, B, etc.). Two experimental quantities, VDE and ADE, are extracted from each spectrum, proving important in establishing a cluster's electronic and geometric structure. VDE is obtained by taking the energy of the peak maximum, and ADE corresponds to an extrapolation of the leading edge of the first peak (band X) in each spectrum. The measured detachment energies, the anisotropy parameters (β), and calculated detachment energies for the respective transitions are given in Table 2.

4.1.1. Photoelectron Imaging of MgO^-. Figure 1 shows the results of the photoelectron imaging experiments of MgO^- at two different photon energies which are 2.33 eV (532 nm) and 3.49 eV (355 nm). The direction of laser polarization is vertical in the image plane (double yellow arrow). Listed in Table 2 are the ADE, VDEs, and β parameters observed in the photoelectron image and reconstructed binding energy spectrum of MgO^-. The extracted photoelectron spectra for MgO^- at two different photon energies (Figure 1a and b) are in excellent agreement with previous experimental results performed by using magnetic bottle photoelectron spectroscopy.[33,34] As shown in Figure 1, four prominent bands are observed below 3 eV: X (VDE: 1.61 eV), A (1.97 eV), B (∼2.08 eV), and C (2.68 eV). The 532 nm spectrum of MgO^- (Figure 1a) reveals the ground-state detachment transition (X) with discernible vibrational structures and another two well-defined bands (A and B). From the MgO^- spectrum, the electron affinity of the neutral MgO is determined to be around 1.61 eV, which is consistent with previous experimental results.[33,34] The observed three bands (X, A, and B) come from the electronic transitions from the ground state ($X^2\Sigma^+$) of MgO^- to the ground state ($X^1\Sigma^+$) and excited states ($a^3\Pi$, $A^1\Pi$) of neutral MgO, respectively.[33] At higher photon energy (355 nm), a relatively intense and sharp band C is seen at a VDE of 2.68 eV, which corresponds to the $b^3\Sigma^+$ excited states of neutral MgO. There is no appreciable neutral vibrational progression observed in this band, indicating that there is little change in geometry between this state and the anionic ground state. In addition, the β parameters for different transitions were also obtained at two select photon energies. In the case of band X, the photoelectron angular distributions (PADs) are preferably oriented parallel to the laser polarization at both 532 and 355 nm, as shown in Figure 1. The measured β parameters associated with this transition are about 1.20 and 1.12, respectively, which indicates that the photoelectron detachment occurs from a σ molecular orbital.[67] As for transitions A and B, isotropic PADs are clearly observed from the MgO^- images of Figure 1. The β parameters for band A are determined to be β(A) = −0.11 at 532 nm and β(A) = 0.50 at 355 nm, while the β values of −0.27 and 0.36 are obtained for band B at 532 and 355 nm, respectively. It is reasonable that the β parameter of the same transition changes slightly at different photon energies since it is strongly dependent on the kinetic energy of the emitted electrons, which has been demonstrated in the case of the O^- atomic ion.[68] Similar to band X, the PAD of band C, shown in Figure

Table 2. Experimental and Theoretical Adiabatic Detachment Energies (ADE) and Vertical Detachment Energies (VDE), in Units of eV, for the MgO_x^- (x = 1−4) Clusters[a]

		VDE			ADE			β parameter[c]	
		exp.			exp.				
species	band	532 nm	355 nm	theor.[b]	532 nm	355 nm	theor.[b]	532 nm	355 nm
$^2MgO^-$	X	1.61(3)	1.61(7)	1.62	1.61(3)	1.61(7)	1.60	1.20(8)	1.12(6)
	A	1.97(2)	1.97(9)	1.88				−0.11(2)	0.50(5)
	B	2.09(2)	2.08(6)					−0.27(3)	0.36(1)
	C		2.68(5)						1.13(5)
$^2MgO_2^-$	X	2.26(10)	2.22(9)	2.10	1.91(4)	1.89(5)	2.05	−0.10(2)	0.32(9)
	A		2.98(10)	2.85					0.33(12)
$^2MgO_3^-$	X	2.26(7)	2.10(8)	2.17	1.98(9)	1.97(3)	2.01	−0.05(2)	0.25(3)
	A		2.97(9)	2.81					0.06(8)
$^2MgO_4^-$	X	2.02(16)		2.08	1.62(7)		1.76	−0.02(3)	
	A	2.25(9)		2.20				−0.05(3)	

[a]For theoretical VDEs, transitions to both the lower (M − 1) and higher (M + 1) spin states are listed when appropriate. Numbers in the parentheses represent experimental uncertainties in the last digits. [b]The theoretical VDE and ADE values are obtained at the CCSD(T)/aug-cc-PVQZ level of theory by refining the total energy of ground state structures which are optimized at the PBEPBE/aug-cc-PVQZ level of theory. [c]Experimental anisotropy parameters (β) for MgO_x^- (x = 1−4) clusters.

1b, also presents preferential parallel distribution with respect to the laser polarization. A β value of 1.13 is observed which is almost equal to that of band X, indicating that the detachment process occurs from a molecular orbital composed mainly of the σ orbital.

4.1.2. Photoelectron Imaging of MgO_2^-. The results of the photoelectron imaging experiments of MgO_2^- acquired using photons of 532 and 355 nm, respectively, are presented in Figure 2. As shown in Figure 2a, only one primary peak (X) is accessible using the 2.33 eV photon energy, representing the transition from the electronic ground state of MgO_2^- to the corresponding neutral electronic ground state. The VDE for this transition is determined to be 2.26 eV. A weak shoulder (X′) located at around 1.46 eV is also observed in the 532 nm spectrum, likely due to a minor isomer of MgO_2^- because it becomes negligible in the high photon energy spectrum.[69] The ADE of MgO_2^-, which is about 1.91 eV, is obtained by extrapolating the leading edge of band X, which could provide a valid estimation of the true ADE when the vibrational progression is not well-resolved.[70,71] As shown in Figure 2a, the PAD of transition X resulting from the detachment of the HOMO (highest occupied molecular orbital) is nearly isotopic, and the β value is measured to be −0.10 indicating that the detachment process arises from molecular orbital of a mainly p-type character. Furthermore, the 355 nm spectrum of MgO_2^- (Figure 2b) reveals a new band (A) which is located at 2.98 eV. Band A is less intense than band X, and the corresponding β parameter for this transition is around 0.33, which is listed in Table 2.

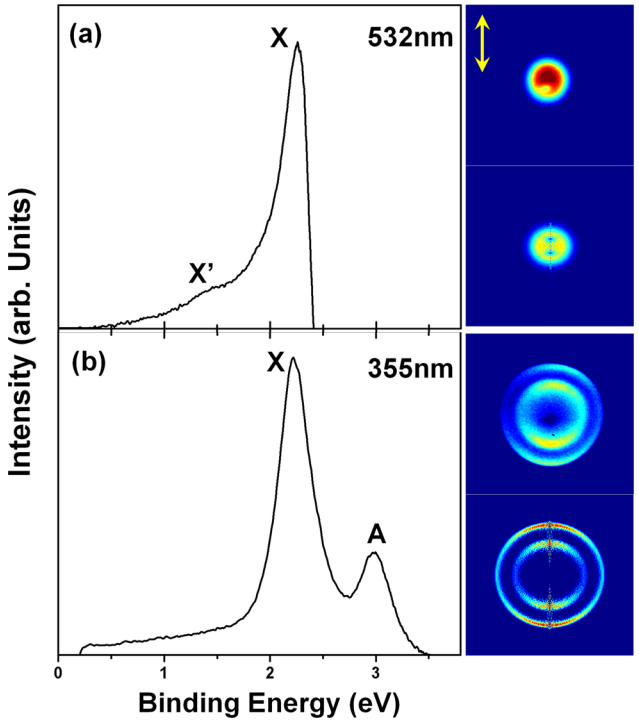

Figure 2. Photoelectron raw images (top on the right), reconstructed images (bottom on the right), and the photoelectron spectra of MgO_2^- obtained at (a) 532 nm (2.33 eV) and (b) 355 nm (3.49 eV). Laser polarization is vertical in the plane of the page.

4.1.3. Photoelectron Imaging of MgO_3^-. Figure 3 depicts the photoelectron images and corresponding binding energy (BE) spectra obtained for MgO_3^- using 532 and 355 nm photons. As shown in Figure 3, two prominent peaks, labeled X and A, are observed below 3.49 eV. Peak X is noted as the electron affinity defining transition and a VDE of 2.18 eV (the averaged value of 2.26 and 2.10 eV for experimental results at both wavelengths) is determined. The electron affinity of MgO_3 is evaluated to be 1.98 eV from the reasonably well-defined onset of band X in the 532 nm spectrum. Similar to the 532 nm spectrum of MgO_2^-, a small shoulder (X′) has also been found in the lower binding energy region of 532 nm spectrum of MgO_3^-. Band X of MgO_3^- arising from electron detachment from the HOMO presents an isotropic angular distribution, and the β parameter is measured to be −0.05 in the 532 nm experiment. Another feature, marked as A in the 355 nm spectrum, is observed at around 2.97 eV, defining an X−A energy gap of ∼0.79 eV. The PAD is nearly isotropic for this transition, and a β value of 0.06 indicates that the detachment occurs from a molecular orbital composed mainly of the p-type character.

4.1.4. Photoelectron Imaging of MgO_4^-. Figure 4 presents our results for MgO_4^- obtained at 532 nm photon energy only.

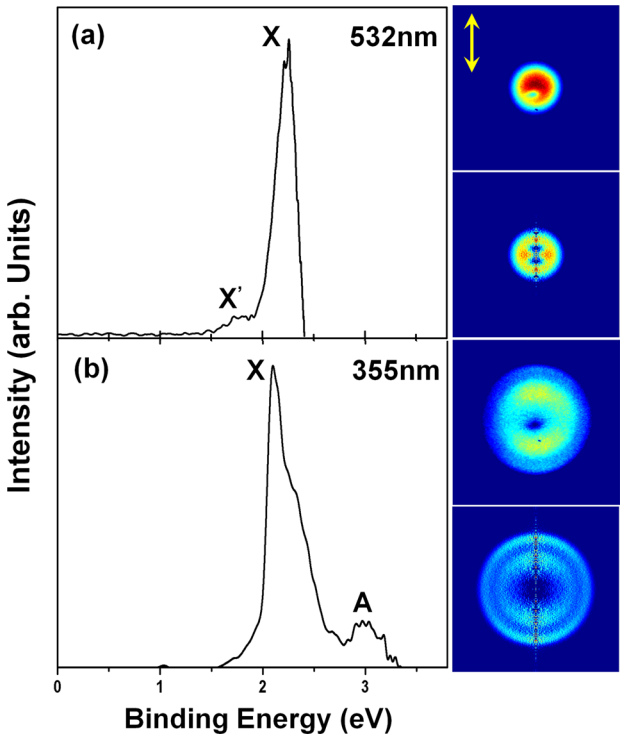

Figure 3. Photoelectron raw images (top on the right), reconstructed images (bottom on the right), and the photoelectron spectra of MgO_3^- obtained at (a) 532 nm (2.33 eV) and (b) 355 nm (3.49 eV). Laser polarization is vertical in the plane of the page.

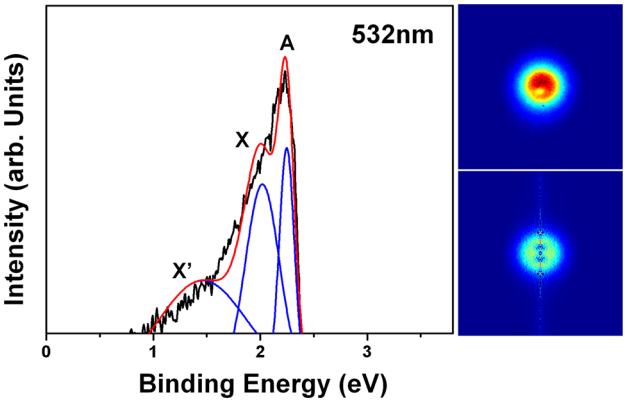

Figure 4. Photoelectron raw image (top on the right), reconstructed image (bottom on the right), and the photoelectron spectrum of MgO_4^- obtained at 532 nm (2.33 eV). Laser polarization is vertical in the plane of the page.

It is worth noting that the intensity of the cluster MgO_4^- in the mass spectrum is much lower than that of the three other smaller clusters, a finding which may be an indication of reduced stability. The weak ion signal intensity also prevented us from collecting the photoelectron image of MgO_4^- at 355 nm because of a lower signal to background electrons ratio. As shown in Figure 4, the photoelectron spectrum of MgO_4^- at 532 nm is not well-resolved due to the low intensity of ion signal. However, three features can still be observed, marked as X′, X, and A, in the spectrum. Here, the multi-Gaussian fits method based on the Gaussian distribution has been used to determine the peak positions in the spectrum. The ADE for MgO_4^- is determined to be 1.62 eV, and its first VDE value is about 2.02 eV. Additionally, the VDE associated with band A is evaluated to be around 2.25 eV. The PADs for transitions X and A, as shown in Figure 4, are both isotropic, and corresponding β parameters are listed in Table 2. Interestingly, the experimental ADE value for MgO_4^- is much lower than that of the MgO_2^- and MgO_3^-. In general, a low ADE signifies stability of the neutral, as it is "easy" to remove an electron from the anion. Such a variation in ADE, therefore, may indicate an enhanced stability in neutral MgO_4. However, we are unable to draw any strong conclusion about the relative stability in neutral MgO_x clusters just from this alone. We will also consult other pieces of evidence to investigate the relative stability of neutral and anionic MgO_x clusters in section 4.4.

4.2. Electronic Structure Calculations on Neutral and Anionic MgO_x (x = 1−4) Clusters. Figure 5 presents the optimized geometries of MgO_x and MgO_x^- (x = 1−4) clusters and some low-lying isomers calculated at the PBEPBE/aug-cc-pVQZ level of theory. In the figure, the bond lengths, bond angles, relative energies (ΔE_R) with respect to the ground state, and spin multiplicities for anionic and neutral clusters are summarized. The equilibrium bond lengths of MgO and MgO^- clusters are calculated to be 1.751 and 1.805 Å, respectively. There is a slight elongation (∼ 0.05 Å) of the monoxide Mg−O bond length on going from MgO to MgO^-. Concurrently, the calculated vibrational frequencies decrease by about 100 cm^{-1} (see Table 1). The spin multiplicities of MgO and MgO^- clusters are 1 and 2, respectively, which agree with the results reported by other experimental[62] and theoretical[58] groups.

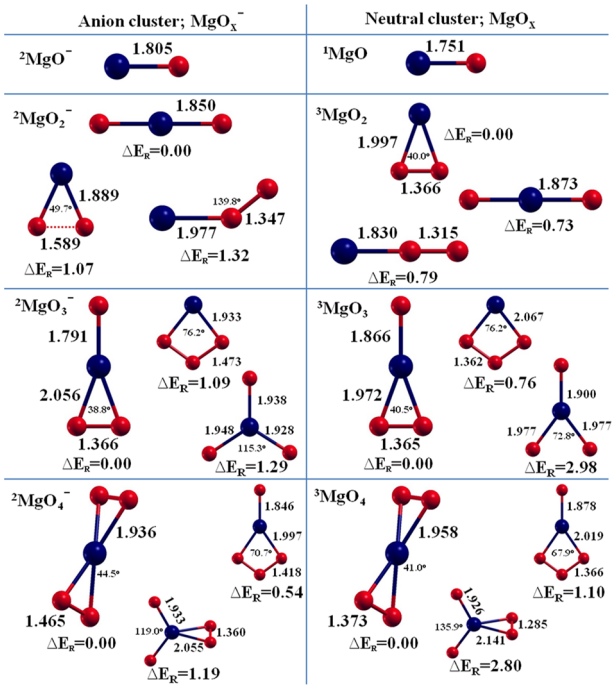

Figure 5. Optimized geometries of the low-lying states of anionic (left side) and neutral (right side) MgO_x (x = 1−4) clusters determined at the PBEPBE/aug-cc-pVQZ level of theory. Bond lengths are given in angstroms (Å), and spin multiplicities are denoted as a superscript. The relative energies ΔE_R to the ground state are shown in electronvolts (eV). The red and blue spheres represent oxygen and magnesium atoms, respectively.

The interaction of molecular oxygen with Mg leads to the formation of an oxide $MgO_2^{0/-}$ where O_2 is dissociated to form

dx.doi.org/10.1021/jp403134g | J. Phys. Chem. A 2013, 117, 11896−11905

a dioxide, a peroxide, and a superoxide complex. It is worth noting that peroxide and superoxide are well-defined chemical species, which correspond to O_2^{2-} (~1.49 Å) and O_2^- (~1.33 Å), respectively. In these complexes, the ground state of $^2MgO_2^-$ cluster (ΔE_R = 0.00 eV) is a dioxide form with the Mg−O bond length of 1.850 Å, while the ground state of neutral $^3MgO_2$ (ΔE_R = 0.00 eV) possesses a superoxide unit which is a triangle structure with the bond lengths of Mg−O = 1.997 Å and O−O = 1.366 Å, and the bond angle of ∠OMgO = 40.0° (see Figure 5). Moreover, the select low-lying isomers that belong to MgO_2^- and MgO_2 clusters are demonstrated as well. The peroxide MgO_2^- is one of the low-lying isomers (ΔE_R = 1.07 eV), involving a Mg−O bond length of 1.889 Å and an elongated O_2 unit (1.589 Å), which is a typical peroxide complex. The superoxide MgO_2^- is a higher energy isomer (ΔE_R = 1.32 eV), and the Mg−O bond length is 1.977 Å, which is longer than that in peroxide and dioxide MgO_2^- by 0.09 and 0.13 Å, respectively. Another feature worth mentioning is that the superoxide MgO_2^- has a bent geometry with the ∠MgOO angle being ~140°. The O−O bond length in the superoxide MgO_2^- is 1.347 Å, which indicates that the oxygen atoms form a partial double bond because the bond length between middle and terminal oxygen atoms corresponds to midway between a double O═O bond (1.21 Å) and a single O−O bond (1.45 Å).[50] In the case of neutral MgO_2 clusters, the superoxide MgO_2 is the ground state structure and more stable than the dioxide (ΔE_R = 0.73 eV) and linear-superoxide (ΔE_R = 0.79 eV) complexes.

Figure 5 also depicts the ground state geometries of $^3MgO_3$ and $^2MgO_3^-$ clusters as well as the corresponding low-lying isomers. The oxosuperoxide ($OMg(O_2)$) form of $^3MgO_3$ (ΔE_R = 0.00 eV) has the lowest energy, which is 0.76 and 2.98 eV more stable than the ozonide ($Mg(O_3)$) and trioxide (MgO_3) forms, respectively. In the oxosuperoxide $^3MgO_3$, the bond lengths of O−Mg and Mg−O are 1.866 and 1.972 Å, respectively. The O−O bond length is 1.365 Å, which is comparable to that of the superoxide MgO_2. This indicates that the O−O bond in the oxosuperoxide $^3MgO_3$ still preserves a partial double bond feature. The ground state of $^2MgO_3^-$ is also in the oxosuperoxide form, which has lower energy than that of the ozonide and trioxide forms by 1.09 and 1.29 eV, respectively. The O−Mg and Mg−O bond lengths in the oxosuperoxide $^2MgO_3^-$ are 0.075 Å shorter and 0.084 Å longer, respectively, than that of the neutral counterpart. The $^3MgO_3$ cluster has a triplet spin multiplicity while it is doublet spin multiplicity for the $^2MgO_3^-$ cluster. It is worth noting that the active oxygen units, $O_2^•$ superoxide with the O−O bond length of ~1.366 Å, appear in both the anionic and neutral oxosuperoxide MgO_3 clusters, which may indicate a special chemical reactivity of these clusters.[27−30]

In addition, the optimized geometries of the anionic and neutral MgO_4 clusters are also displayed in Figure 5. The ground state structures of the $MgO_4^{0/-}$ clusters contain two molecular O_2 units, respectively. The relative energy of the ground-state $^3MgO_4$ cluster (ΔE_R = 0.00 eV) is 1.10 and 2.80 eV lower than that of the two low-lying isomers, which are $OMg(O_3)$ and $OOMg(O_2)$, respectively. In $OMg(O_3)$, an additional O atom is bonded to the ozonide MgO_3 with the O−Mg bond length of 1.878 Å. As for $OOMg(O_2)$, the O−O and O−Mg bond lengths are 1.285 Å and 2.141 Å, respectively, and the bond angle of ∠OMgO is around 34.9°, whereas another two oxygen atoms are attached dissociatively in $OOMg(O_2)$ with the O−Mg bond length of 1.926 Å. In the case of anionic forms, the ground-state geometry and the low-lying isomers of $^2MgO_4^-$ clusters are similar to those of the neutral $^3MgO_4$ ones.

4.3. Comparison between Experiment and Theory. The PES bands in Figures 1−4 serve as an electronic fingerprint for the MgO_x^- (x = 1−4) clusters, allowing comparison with theoretical calculations to validate optimized global minimum structures. As mentioned above, two experimental quantities, which are ADE and VDE, respectively, could be extracted from each photoelectron spectrum. These quantities can also be reproduced based on the optimized ground-state geometries of the studied clusters provided in Figures 5. As previously noted, there is only one ADE for each cluster, while there can be multiple VDEs, which correspond to different resolved peaks in the spectrum. The calculated ADE values are obtained as the energy difference between the anion and neutral in their respective ground state geometries. Meanwhile, the theoretical VDEs are calculated by taking the energy difference between the ground-state geometry of the anion with multiplicity M and the neutral cluster with the anion geometry in $M \pm 1$ multiplicity states. The experimental and theoretical ADE and VDEs for the MgO_x^- (x = 1−4) clusters are listed in Table 2. Both the $M - 1$ (singlet) and the $M + 1$ (triplet) VDE are listed theoretically since all the optimized ground-state MgO_x^- (x = 1−4) clusters have doublet spin multiplicity, and these two-peak features are also observed in our experimental spectra, which are marked as X and A bands in Figures 1−4. In addition, there are two additional VDEs (bands B and C) in the spectrum of MgO^-, which are results of the removal of deeper lying electrons leading to the neutral cluster in excited states. As shown in Table 2, the experimental and theoretical results of ADE and VDEs for MgO_x^- (x = 1−4) are in good agreement. For example, in the case of MgO_2^-, the experimental VDEs for bands X and A in the 355 nm spectrum are 2.22 and 2.98 eV, respectively, which are very close to the theoretical values of 2.10 and 2.85 eV. Additionally, the ADE is measured to be around 1.89 eV at 355 nm, which is consistent with the calculated value of 2.05 eV. Therefore, the agreement between experiment and theory gives us confidence that the calculated ground-state structures shown in Figure 5 are correct.

4.4. Stability Analyses of the Anionic and Neutral MgO_x (x = 1−4) Clusters. To investigate the relative stabilities of the anionic and neutral MgO_x (x = 1−4) clusters studied here, we consult multiple pieces of evidence. The first one is the averaged binding energies of atomic oxygen to the magnesium (BE_O), which can be defined as the following formula

$$BE_O^{0/-} = [E(Mg^{0/-}) + xE(O) - E(MgO_x^{0/-})]/x \quad (2)$$

where $E(Mg^{0/-})$, $E(O)$, and $E(MgO_x^{0/-})$ are the total energies of most stable $Mg^{0/-}$, O, and $MgO_x^{0/-}$ species, respectively. The calculated BE_O are plotted as curves, showing the size dependence of the averaged binding energies of $MgO_x^{0/-}$ (x = 1−4) clusters, which are depicted in Figure 6. In the case of neutral MgO_x clusters, the BE_O rises almost uniformly from MgO to MgO_4. This means that the amount of energy required to dissociate the MgO_4 cluster into their respective atoms is higher than that of the MgO_x (x = 1−3) clusters. Accordingly, the MgO_4 neutral cluster is found to have an enhanced relative stability in this series. In the series of anionic clusters, further increasing the number of oxygen atoms in the MgO_x^- clusters (x = 1−4) is not energetically favorable in BE_O. Therefore, the

dx.doi.org/10.1021/jp403134g | J. Phys. Chem. A 2013, 117, 11896−11905

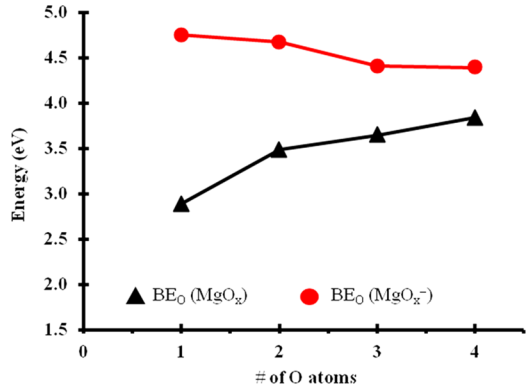

Figure 6. Size dependence of the averaged binding energies of atomic oxygen in $MgO_x^{0/-}$ (x = 1−4) clusters.

MgO^- is shown to have a large relative stability, which can be seen from Figure 6.

In addition, the energetic and chemical stabilities of the anionic and neutral MgO_x (x = 1−4) clusters are further investigated by considering the energy gain and the gap between the highest occupied molecular orbital (HOMO) and the lowest unoccupied molecular orbital (LUMO), which are shown in Figure 7. As an indicator of the energetic stability, the

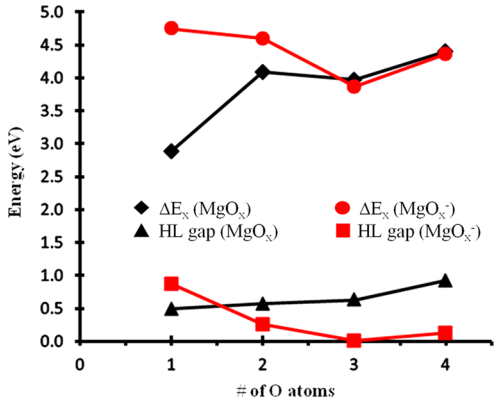

Figure 7. Size dependence of the energy gain of atomic oxygen in $MgO_x^{0/-}$ (x = 1−4) clusters and the HOMO−LUMO gap trends.

gain in energy $\Delta E_x^{0/-}$ can be taken into account when successive oxygen atoms bind to a neutral or anionic Mg atom, and it can be calculated by the formula given below

$$\Delta E_x^{0/-} = E(MgO_{x-1}^{0/-}) + E(O) - E(MgO_x^{0/-}) \quad (3)$$

where $E(MgO_{x-1}^{0/-})$ is the total energy of the most stable $MgO_{x-1}^{0/-}$ species. A higher energy gain is an indicator of stability when a cluster forms from a stoichiometry with one less atom. The HOMO−LUMO gap is calculated as a quantitative characteristic of the cluster's chemical stability. Generally, the clusters with larger HOMO−LUMO gaps are more stable and chemically inert. As shown in Figure 7, the MgO_4 cluster in the series of neutral clusters and the MgO^- cluster in the series of anionic clusters have higher energy gain than their neighboring clusters. Additionally, the HOMO−LUMO gaps for the neural MgO_x (x = 1−4) clusters are calculated to be about 0.49, 0.57, 0.63, and 0.92 eV, respectively. In the case of anionic series, the calculated gaps are around 0.87, 0.26, 0.01, and 0.13 eV, which are shown in Figure 7 schematically. It is obvious that the MgO_4 and MgO^- clusters have the largest HOMO−LUMO gaps of 0.92 and 0.87 eV, respectively, among the neutral and anionic clusters studied here, indicating that these clusters should have weaker chemical reactivity than their neighbors. Interestingly, the MgO_3 cluster has the lowest HOMO−LUMO gap of 0.01 eV, and it should be chemically reactive which means that the electrons in the MgO_3 cluster are relatively easier to be excited.

Furthermore, to gain more insights into the stability of the clusters studied here, we have analyzed the fragmentation behavior, providing the thermodynamic stability, of the anionic and neutral MgO_x (x = 1−4) clusters for various dissociation pathways. Investigating such stability can provide insights into viable pathways for synthesizing cluster-assembled materials from potential building blocks.[72] The fragmentation energy E_f is defined as the difference in total energies between the reactant and the products formed in a particular decay channel

$$E_f = E(MgO_{x-y}^{0/-}) + E(O_y^{0/-}) - E(MgO_x^{0/-}) \quad (4)$$

with y = 1 and 2. We can consider clusters with large positive E_f to be more stable and those with slightly positive E_f to be unstable as they are more easily dissociated. We have calculated major fragmentation channels that involve monatomic Mg and O, diatomic MgO and O_2, triatomic MgO_2, tetraatomic MgO_3, and their anions as products. The results are presented in Table 3 and compared with the available experimental data on

Table 3. Fragmentation Energies (E_f in eV) of MgO_x and MgO_x^- (x = 1−4) Clusters Computed According to Equation 4

Neutral MgO_x		Anionic MgO_x	
Fragmentation Channel	E_f (eV)	Fragmentation Channel	E_f (eV)
$MgO \leftrightarrow Mg+O$	2.88[a]	$MgO^- \leftrightarrow Mg+O^-$	2.96
		$\leftrightarrow Mg^-+O$	4.75
$MgO_2 \leftrightarrow Mg+O_2$	1.35	$MgO_2^- \leftrightarrow Mg+O_2^-$	2.75
$\leftrightarrow MgO+O$	4.09	$\leftrightarrow Mg^-+O_2$	3.20
		$\leftrightarrow MgO+O^-$	4.75
		$\leftrightarrow MgO^-+O$	4.61
$MgO_3 \leftrightarrow MgO+O_2$	2.54	$MgO_3^- \leftrightarrow MgO+O_2^-$	3.74
$\leftrightarrow MgO_2+O$	3.98	$\leftrightarrow MgO^-+O_2$	2.84
		$\leftrightarrow MgO_2+O^-$	4.46
		$\leftrightarrow MgO_2^-+O$	3.87
$MgO_4 \leftrightarrow MgO_2+O_2$	3.02	$MgO_4^- \leftrightarrow MgO_2+O_2^-$	4.18
$\leftrightarrow MgO_3+O$	4.40	$\leftrightarrow MgO_2^-+O_2$	2.08
		$\leftrightarrow MgO_3+O^-$	5.07
		$\leftrightarrow MgO_3^-+O$	4.33

[a]The calculated value is consistent with the experimental[73] result of 2.56 eV.

MgO.[73] In the neutral cluster series, we can see a gradual increase in fragmentation energies required for dissociation to O_2 with increasing x (x = 2−4), and the energies required to release O_2 are about 1.4−2.7 eV smaller than those for the release of atomic oxygen. This result implies that, in the case of MgO_x (x = 2−4), the most favorable dissociation channel

dx.doi.org/10.1021/jp403134g | J. Phys. Chem. A 2013, 117, 11896−11905

corresponds to the production of the O_2 but not an oxygen atom. Furthermore, as shown in Figure 5, the Mg−O bond lengths in MgO_x (x = 2−4) clusters are at least 0.2 Å longer than that in the MgO cluster, indicating that molecular oxygen weakly binds to the Mg atom in MgO_x (x = 2−4) clusters, and can be easily released. Comparing the most favorable decay channel in each neutral MgO_x clusters, our calculations predict that the MgO_4 cluster is thermodynamically more stable. Similarly, in the anionic cluster series, the fragmentation channels leading to the formation of neutral or anionic O_2 are energetically favorable than those to release the neutral or anionic oxygen atom. Looking at the most favorable paths to break each anionic MgO_x (x = 1−4) clusters, MgO^- cluster is the most stable one, and it will not be easily fragmented into Mg and O^-. Overall, based on our present calculations for the fragmentation behavior, MgO_4 and MgO^- clusters are suggested to be more stable in the respective neutral and anionic series, which is in accordance with our BE_O, energy gain, and HOMO−LUMO gap results mentioned earlier.

According to the discussion above, it seems that MgO_4 and MgO^- clusters have enhanced relative stability in the corresponding neutral and anionic cluster series studied here, respectively. Such a finding can be further supported by the collected mass spectrum of the MgO_x^- (x = 1−4) clusters synthesized in our laser vaporization source, which is presented in Figure 8. As evidenced in the cluster distribution, the intensity of the anionic clusters gradually decreases with increasing the cluster size. MgO^- is consistently the most intense peak in the spectrum, indicating an enhanced stability. Additionally, the apparent lack of MgO_4^- production could be explained with the enhanced relative stability of the neutral MgO_4 in the MgO_x series, which has been demonstrated by the discussion above.

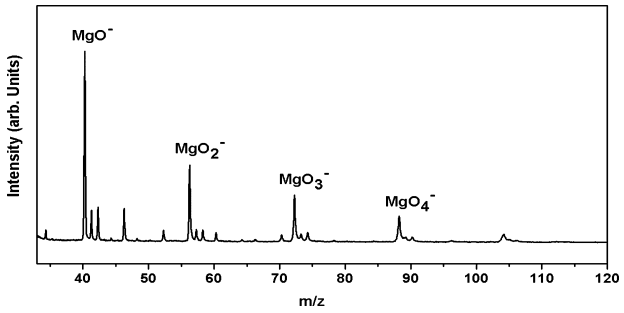

Figure 8. Time-of-flight mass spectrum of MgO_x^- (x = 1−4) cluster anions.

5. CONCLUSIONS

In the present study, the electronic and structural properties of neutral and negatively charged MgO_x (x = 1−4) clusters were investigated by combining photoelectron imaging spectroscopy and first principles calculations. The electron affinities for the neutral MgO_x (x = 1−4) clusters have been determined experimentally, which are about 1.61, 1.91, 1.98, and 1.62 eV, respectively. The photoelectron angular distributions of the electrons photodetached from MgO_x^- (x = 1−4) clusters at different photon energies were reported, and they were found to be dependent on both the orbital symmetry and electron kinetic energies. In addition, extensive DFT calculations were performed in search of the lowest energy structures for both the neutral and anionic clusters. The optimized geometries have also been verified according to the good agreement between the experimental and theoretical findings. Moreover, the relative stability of the neutral and anionic MgO_x clusters were investigated by analyzing different criterions, including the BE_O, energy gain, HOMO−LUMO gaps, and also the fragmentation behavior. Based on both theoretical predictions and the experimental mass spectrum, MgO^- and MgO_4 clusters are suggested to have an enhanced relative stability in the respective anionic and neutral series studied here.

AUTHOR INFORMATION

Corresponding Author

*Tel.: (814)865-7242. Fax: (814)865-5235. E-mail address: awc@psu.edu.

Present Address

J.J.M.: Air Force Research Laboratory, Space Vehicles Directorate, Kirtland AFB, New Mexico, 87117−5776, United States.

Notes

The authors declare no competing financial interest.

ACKNOWLEDGMENTS

We gratefully acknowledge funding from the Office of Naval Research (ONR) Grant N00014-12-1-0541.

REFERENCES

(1) Jena, P.; Rao, B. K.; Khanna, S. N., Eds. *Physics and Chemistry of Small Clusters*; Plenum Press: New York, 1987.
(2) Khanna, S. N.; Castleman, A. W., Jr., Eds. *Quantum Phenomena in Clusters and Nanostructures*; Springer: Germany, 2003.
(3) Mark, T. D.; Castleman, A. W., Jr. Experimental Studies on Cluster Ions. *Adv. Atomic Mol. Phys.* **1985**, *20*, 65−172.
(4) Castleman, A. W., Jr.; Keesee, R. G. Clusters: Bridging the Gas and Condensed Phases. *Acc. Chem. Res.* **1986**, *19*, 413−419.
(5) Castleman, A. W., Jr.; Keesee, R. G. Gas-Phase Clusters: Spanning the States of Matter. *Science* **1988**, *241*, 36−42.
(6) Castleman, A. W., Jr.; Keesee, R. G. Ionic Clusters. *Chem. Rev.* **1986**, *86*, 589−618.
(7) Castleman, A. W., Jr.; Jena, P. Clusters: A Bridge between Disciplines. *Proc. Natl. Acad. Sci. U.S.A.* **2006**, *103*, 10552−10553.
(8) Castleman, A. W., Jr.; Jena, P. Clusters: A Bridge across the Disciplines of Environment, Materials Science, and Biology. *Proc. Natl. Acad. Sci. U.S.A.* **2006**, *103*, 10554−10559.
(9) Jena, P.; Castleman, A. W., Jr. Clusters: A Bridge across the Disciplines of Physics and Chemistry. *Proc. Natl. Acad. Sci. U.S.A.* **2006**, *103*, 10560−10569.
(10) Nasibulin, A. G.; Sun, L.; Hamalainen, S.; Shandakov, S. D.; Banhart, F.; Kauppinen, E. I. In Situ TEM Observation of MgO Nanorod Growth. *Cryst. Growth Des.* **2010**, *10*, 414−417.
(11) Hu, J. Q.; Li, Q.; Meng, X. M.; Lee, C. S.; Lee, S. T. Thermal Reduction Route to the Fabrication of Coaxial Zn/ZnO Nanocables and ZnO Nanotubes. *Chem. Mater.* **2002**, *15*, 305−308.
(12) Xu, J. Q.; Chen, Y. P.; Li, Y. D.; Shen, J. N. Gas Sensing Properties of ZnO Nanorods Prepared by Hydrothermal Method. *J. Mater. Sci.* **2005**, *40*, 2919−2921.
(13) Hyeon, T. Chemical Synthesis of Magnetic Nanoparticles. *Chem. Commun.* **2003**, 927−934.
(14) Henrich;, V. E.; Cox, P. A. *The Surface Science of Metal Oxides*; Cambridge University Press: Cambridge, UK, 1994.
(15) Wang, L. L.; Munir, Z. A.; Maximov, Y. M. Thermite Reactions: their Utilization in the Synthesis and Processing of Materials. *J. Mater. Sci.* **1993**, *28*, 3693−3708.
(16) Sterrer, M.; Risse, T.; Pozzoni, U. M.; Giordano, L.; Heyde, M.; Rust, H. P.; Pacchioni, G.; Freund, H. J. Control of the Charge State of Metal Atoms on Thin MgO Films. *Phys. Rev. Lett.* **2007**, *98*, 096107 (4 pages).

(17) Konig, T.; Simon, G. H.; Rust, H. P.; Pacchioni, G.; Heyde, M.; Freund, H. J. Measuring the Charge State of Point Defects on MgO/Ag(001). *J. Am. Chem. Soc.* **2009**, *131*, 17544−17545.
(18) Freund, H. J.; Pacchioni, G. Oxide Ultra-thin Films on Metals: New Materials for the Design of Supported Metal Catalysts. *Chem. Soc. Rev.* **2008**, *37*, 2224−2242.
(19) Lee, S. C.; Chae, H. J.; Lee, S. J.; Choi, B. Y.; Yi, C. K.; Lee, J. B.; Ryu, C. K.; Kim, J. C. Development of Regenerable MgO-based Sorbent Promoted with K_2CO_3 for CO_2 Capture at Low Temperatures. *Environ. Sci. Technol.* **2008**, *42*, 2736−2741.
(20) Xiao, G. K.; Singh, R.; Chaffee, A.; Webley, P. Advanced Adsorbents based on MgO and K_2CO_3 for Capture of CO_2 at Elevated Temperatures. *Int. J. Greenhouse Gas Control* **2011**, *5*, 634−639.
(21) Bhagiyalakshmi, M.; Hemalatha, P.; Ganesh, M.; Mei, P. M.; Jang, H. T. A Direct Synthesis of Mesoporous Carbon Supported MgO Sorbent for CO_2 Capture. *Fuel* **2011**, *90*, 1662−1667.
(22) Dong, F.; Heinbuch, S.; Xie, Y.; Rocca, J. J.; Bernstein, E. R.; Wang, Z. C.; Deng, K.; He, S. G. Experimental and Theoretical Study of the Reactions between Neutral Vanadium Oxide Clusters and Ethane, Ethylene, and Acetylene. *J. Am. Chem. Soc.* **2008**, *130*, 1932−1943.
(23) Huang, X.; Zhai, H. J.; Waters, T.; Li, J.; Wang, L. S. Experimental and Theoretical Characterization of Superoxide Complexes $[W_2O_6(O_2^-)]$ and $[W_3O_9(O_2^-)]$: Models for the Interaction of O_2 with Reduced W Sites on Tungsten Oxide Surfaces. *Angew. Chem., Int. Ed.* **2006**, *45*, 657−660.
(24) Zhai, H. J.; Zhang, X. H.; Chen, W. J.; Huang, X.; Wang, L. S. Stoichiometric and Oxygen-Rich $M_2O_n^-$ and M_2O_n (M = Nb, Ta; n = 5−7) Clusters: Molecular Models for Oxygen Radicals, Diradicals, and Superoxides. *J. Am. Chem. Soc.* **2011**, *133*, 3085−3094.
(25) Zhai, H. J.; Kiran, B.; Cui, L. F.; Li, X.; Dixon, D. A.; Wang, L. S. Electronic Structure and Chemical Bonding in MO_n^- and MO_n Clusters (M = Mo, W; n = 3−5): A Photoelectron Spectroscopy and ab Initio Study. *J. Am. Chem. Soc.* **2004**, *126*, 16134−16141.
(26) Zhai, H. J.; Wang, L. S. Probing the Electronic Structure and Band Gap Evolution of Titanium Oxide Clusters $(TiO_2)_n^-$ (n = 1−10) Using Photoelectron Spectroscopy. *J. Am. Chem. Soc.* **2007**, *129*, 3022−3026.
(27) Justes, D. R.; Mitrić, R.; Moore, N. A.; Bonačić-Koutecký, V.; Castleman, A. W., Jr. Theoretical and Experimental Consideration of the Reactions between $V_xO_y^+$ and Ethylene. *J. Am. Chem. Soc.* **2003**, *125*, 6289−6299.
(28) Johnson, G. E.; Mitrić, R.; Tyo, E. C.; Bonačić-Koutecký, V.; Castleman, A. W., Jr. Stoichiometric Zirconium Oxide Cations as Potential Building Blocks for Cluster Assembled Catalysts. *J. Am. Chem. Soc.* **2008**, *130*, 13912−13920.
(29) Johnson, G. E.; Mitrić, R.; Nössler, M.; Tyo, E. C.; Bonačić-Koutecký, V.; Castleman, A. W., Jr. Influence of Charge State on Catalytic Oxidation Reactions at Metal Oxide Clusters Containing Radical Oxygen Centers. *J. Am. Chem. Soc.* **2009**, *131*, 5460−5470.
(30) Nößler, M.; Mitrić, R.; Bonačić-Koutecký, V.; Johnson, G. E.; Tyo, E. C.; Castleman, A. W., Jr. Generation of Oxygen Radical Centers in Binary Neutral Metal Oxide Clusters for Catalytic Oxidation Reactions. *Angew. Chem., Int. Ed.* **2010**, *49*, 407−410.
(31) Gunaratne, K. D. D.; Berkdemir, C.; Harmon, C. L.; Castleman, A. W., Jr. Investigating the Relative Stabilities and Electronic Properties of Small Zinc Oxide Clusters. *J. Phys. Chem. A* **2012**, *116*, 12429−12437.
(32) Molek, K. S.; Jaeger, T. D.; Duncan, M. A. Photodissociation of Vanadium, Niobium, and Tantalum Oxide Cluster Cations. *J. Chem. Phys.* **2005**, *123*, 144313 (10 pages).
(33) Kim, J. H.; Li, X.; Wang, L. S.; de Clercq, H. L.; Fancher, C. A.; Thomas, O. C.; Bowen, K. H. Vibrationally Resolved Photoelectron Spectroscopy of MgO^- and ZnO^- and the Low-lying Electronic States of MgO, MgO^-, and ZnO. *J. Phys. Chem. A* **2001**, *105*, 5709−5718.
(34) Gutowski, M.; Skurski, P.; Li, X.; Wang, L. S. $(MgO)_n^-$ (n = 1−5) Clusters: Multipole-bound Anions and Photodetachment Spectroscopy. *Phys. Rev. Lett.* **2000**, *85*, 3145−3148.
(35) Ziemann, P. J.; Castleman, A. W., Jr. Mass Spectrometric Study of MgO Clusters Produced by the Gas Aggregation Technique. *Z. Phys. D* **1991**, *20*, 97−99.
(36) Ziemann, P. J.; Castleman, A. W., Jr. Stabilities and Structures of Gas-Phase MgO Clusters. *J. Chem. Phys.* **1991**, *94*, 718−728.
(37) van Heijnsbergen, D.; von Helden, G.; Meijer, G.; Duncan, M. A. Infrared Resonance-enhanced Multiphoton Ionization Spectroscopy of Magnesium Oxide Clusters. *J. Chem. Phys.* **2002**, *116*, 2400−2406.
(38) Kwapien, K.; Sierka, M.; Dobler, J.; Sauer, J.; Haertelt, M.; Fielicke, A.; Meijer, G. Structural Diversity and Flexibility of MgO Gas-Phase Clusters. *Angew. Chem., Int. Ed.* **2011**, *50*, 1716−1719.
(39) Roberts, C.; Johnston, R. L. Investigation of the Structures of MgO Clusters Using a Genetic Algorithm. *Phys. Chem. Chem. Phys.* **2001**, *3*, 5024−5034.
(40) Chen, J.; Wong, T. H.; Kleiber, P. D. Photodissociation Spectroscopy of MgO_2^+. *J. Chem. Phys.* **1998**, *109*, 8311−8318.
(41) Yazidi, O.; Ben Houria, A.; Ben Lakhdar, Z.; Senent, M. L.; Hochlaf, M. Electronic Structure and Spectroscopy of the MgO_2^+ Cation. *Chem. Phys.* **2008**, *348*, 215−226.
(42) Knappenberger, K. L.; Jones, C. E.; Sobhy, M. A.; Castleman, A. W., Jr. Versatile Cluster Based Photoelectron Spectrometer. *Rev. Sci. Instrum.* **2006**, *77*, 123901 (8 pages).
(43) Sobhy, M. A.; Reveles, J. U.; Gupta, U.; Khanna, S. N.; Castleman, A. W., Jr. Photoelectron Imaging and Theoretical Investigation of Bimetallic $Bi_{1-2}Ga_{0-2}^-$ and Pb_{1-4}^- Cluster Anions. *J. Chem. Phys.* **2009**, *130*, 054304 (9 pages).
(44) Sobhy, M. A.; Castleman, A. W., Jr. Photoelectron Imaging of Copper and Silver Mono- and Diamine Anions. *J. Chem. Phys.* **2007**, *126*, 154314 (8 pages).
(45) Wiley, W. C.; McLaren, I. H. Time-of-Flight Mass Spectrometer with Improved Resolution. *Rev. Sci. Instrum.* **1955**, *26*, 1150−1157.
(46) Dribinski, V.; Ossadtchi, A.; Mandelshtam, V. A.; Reisler, H. Reconstruction of Abel-transformable Images: The Gaussian Basis-set Txpansion Abel Transform Method. *Rev. Sci. Instrum.* **2002**, *73*, 2634−2642.
(47) Andersen, T.; Haugen, H. K.; Hotop, H. Binding Energies in Atomic Negative Ions: III. *J. Phys. Chem. Ref. Data* **1999**, *28*, 1511−1533.
(48) Frisch, M. J.; Trucks, G. W.; Schlegel, H. B.; Scuseria, G. E.; Robb, M. A.; Cheeseman, J. R.; Scalmani, G.; Barone, V.; Mennucci, B.; Petersson, G. A.; et al. *Gaussian 09*, revision A.1; Gaussian Inc.: Wallingford, CT, 2009.
(49) Gutsev, G. L.; Nooijen, M.; Bartlett, R. J. Valence and Excited Dipole-Bound States of Polar Diatomic Anions: LiH^-, LiF^-, $LiCl^-$, NaH^-, NaF^-, $NaCl^-$, BeO^-, and MgO^-. *Chem. Phys. Lett.* **1997**, *276*, 13−19.
(50) Huber, K. P.; Herzberh, G. *Molecular Spectra and Molecular Structure: Constants of Diatomic Molecules*; Van Nostrand Reinhold: New York, 1979.
(51) Bauschlicher, C. W., Jr.; Partridge, H. On Interpreting the Photoelectron Spectra of MgO^-. *Chem. Phys. Lett.* **2001**, *342*, 441−446.
(52) Becke, A. D. Density-Functional Exchange-Energy Approximation with Correct Asymptotic-Behavior. *Phys. Rev. A: At., Mol., Opt. Phys.* **1988**, *38*, 3098−3100.
(53) Perdew, J. P.; Burke, K.; Ernzerhof, M. Generalized Gradient Approximation Made Simple. *Phys. Rev. Lett.* **1996**, *77*, 3865−3868.
(54) Perdew, J. P.; Kurth, S.; Zupan, A.; Blaha, P. Accurate Density Functional with Correct Formal Properties: A Step Beyond the Generalized Gradient Approximation. *Phys. Rev. Lett.* **1999**, *82*, 2544−2547.
(55) McLean, A. D.; Chandler, G. S. Contracted Gaussian-Basis Sets for Molecular Calculations. I. Second Row Atoms, Z = 11−18. *J. Chem. Phys.* **1980**, *72*, 5639−5648.
(56) Dunning, T. H., Jr. Gaussian Basis Sets for Use in Correlated Molecular Calculations. I. The Atoms Boron through Neon and Hydrogen. *J. Chem. Phys.* **1989**, *90*, 1007−1023.

(57) Woon, D. E.; Dunning, T. H., Jr. Gaussian Basis Sets for Use in Correlated Molecular Calculations. III. The Atoms Aluminum through Argon. *J. Chem. Phys.* **1993**, *98*, 1358−1371.
(58) Schamps, J.; Lefebvre-Brion, H. SCF Calculations of the Electronic States of Magnesium Monoxide. *J. Chem. Phys.* **1972**, *56*, 573−585.
(59) Thümmel, H.; Klotz, R.; Peyerimhoff, S. D. The Electronic Structure of the MgO Molecule in Ground and Excited States. *Chem. Phys.* **1989**, *129*, 417−430.
(60) Bauschlicher, C. W.; Silver, D. M.; Yarkony, D. R. An SCF and MCSCF Description of the Low-Lying States of MgO. *J. Chem. Phys.* **1980**, *73*, 2867−2870.
(61) García Cuesta, I.; Sánchez de Merás, A.; Nebot Gil, I. A MRCI PS and CASSCF Study of the Ground State MgO Dissociation Energy. *Chem. Phys. Lett.* **1991**, *186*, 386−392.
(62) Ikeda, T.; Wong, N. B.; Harris, D. O.; Field, R. W. Argon Ion and Dye Laser Induced MgO $B^1\Sigma^+$-$X^1\Sigma^+$ and $B^1\Sigma^+$-$A^1\Pi$ Photoluminescence Spectra: Analysis of $a^3\Pi_i \sim X^1\Sigma^+$ perturbations. *J. Mol. Spectrosc.* **1977**, *68*, 452−487.
(63) Mürtz, P.; Thümmel, H.; Pfelzer, C.; Urban, W. New Bands of the MgO $A^1\Pi$-$X^1\Sigma^+$ and $a^3\Pi_{0,1}$-$X^1\Sigma^+$ Systems by Faraday Laser Magnetic Resonance Spectroscopy. *Mol. Phys.* **1995**, *86*, 513−534.
(64) Ip, P. C. F.; Cross, K. J.; Field, R. W.; Rostas, J.; Bourguignon, B.; McCombie, J. The $B^1\Sigma^+$-$a^3\Pi_i$ and $D^1\Delta$-$a^3\Pi_1$ Intercombination Systems of the MgO Molecule. *J. Mol. Spectrosc.* **1991**, *146*, 409−436.
(65) Scuseria, G. E.; Janssen, C. L.; Schaefer, H. F. An Efficient Reformulation of the Closed-Shell Coupled Cluster Single and Double Excitation (CCSD) Equations. *J. Chem. Phys.* **1988**, *89*, 7382−7387.
(66) Scuseria, G. E.; Schaefer, H. F. Is Coupled Cluster Singles and Doubles (CCSD) More Computationally Intensive than Quadratic Configuration Interaction (QCISD)? *J. Chem. Phys.* **1989**, *90*, 3700−3703.
(67) Bartels, C. Ph.D. Dissertation, Albert Ludwig University of Freiburg, Freiburg, Germany, 2008.
(68) Hanstorp, D.; Bengtsson, C.; Larson, D. J. Angular Distributions in Photodetachment from O^-. *Phys. Rev. A: At., Mol., Opt. Phys.* **1989**, *40*, 670−675.
(69) Zhai, H. J.; Wang, B.; Huang, X.; Wang, L. S. Probing the Electronic and Structural Properties of the Niobium Trimer Cluster and Its Mono- and Dioxides: $Nb_3O_n^-$ and Nb_3O_n (n = 0−2). *J. Phys. Chem. A* **2009**, *113*, 3866−3875.
(70) Melko, J. J.; Ong, S. V.; Gupta, U.; Reveles, J. U.; D'Emidio, J.; Khanna, S. N.; Castleman, A. W., Jr. Anion Photoelectron Spectroscopy and First-Principles Study of Pb_xIn_y Clusters. *J. Phys. Chem. C* **2010**, *114*, 20907−20916.
(71) Gupta, U.; Reveles, J. U.; Melko, J. J.; Khanna, S. N.; Castleman, A. W., Jr. Origins of Stability in Mixed Bismuth-Indium Clusters. *J. Phys. Chem. C* **2010**, *114*, 15963−15972.
(72) Castleman, A. W., Jr.; Khanna, S. N. Clusters, Superatoms, and Building Blocks of New Materials. *J. Phys. Chem. C* **2009**, *113*, 2664−2675.
(73) Operti, L.; Tews, E. C.; MacMahon, T. J.; Freiser, B. S. Thermochemical Properties of Gas-Phase MgOH and MgO Determined by Fourier Transform Mass Spectrometry. *J. Am. Chem. Soc.* **1989**, *111*, 9152−9156.